ISSN 0006-2979, Biochemistry (Moscow), 2011, Vol. 76, No. 10, pp. 1107-1119. © Pleiades Publishing, Ltd., 2011.
Published in Russian in Biokhimiya, 2011, Vol. 76, No. 10, pp. 1359-1373.
Originally published in Biochemistry (Moscow) On-Line Papers in Press, as Manuscript BM11-121, September 4, 2011.

Coherent Phenomena of Charge Separation in Reaction Centers of LL131H and LL131H/LM160H/FM197H Mutants of *Rhodobacter sphaeroides*

A. G. Yakovlev[1]*, L. G. Vasilieva[2], A. Y. Shkuropatov[2], and V. A. Shuvalov[1,2]

[1]*Department of Photobiophysics, Belozersky Institute of Chemical and Physical Biology, Lomonosov Moscow State University, 119991 Moscow, Russia; fax: (495) 939-3181; E-mail: yakov@genebee.msu.su*
[2]*Institute of Basic Biological Problems, Russian Academy of Sciences, 142290 Pushchino, Moscow Region, Russia; fax: (496) 773-0532; E-mail: shuvalov@issp.serpukhov.su*

Received April 18, 2011
Revision received May 19, 2011

Abstract—Primary stage of charge separation and transfer of charges was studied in reaction centers (RCs) of point mutants LL131H and LL131H/LM160H/FM197H of the purple bacterium *Rhodobacter sphaeroides* by differential absorption spectroscopy with temporal resolution of 18 fsec at 90 K. Difference absorption spectra measured at 0-4 psec delays after excitation of dimer P at 870 nm with 30 fsec step were obtained in the spectral range of 935-1060 nm. It was found that a decay of P* due to charge separation is considerably slower in the mutant RCs in comparison with native RCs of *Rba. sphaeroides*. Coherent oscillations were found in the kinetics of stimulated emission of the P* state at 940 nm. Fourier analysis of the oscillations revealed a set of characteristic bands in the frequency range of 20-500 cm^{-1}. The most intense band has the frequency of ~130 cm^{-1} in RCs of mutant LL131H and in native RCs and the frequency of ~100 cm^{-1} in RCs of the triple mutant. It was found that an absorption band of bacteriochlorophyll anion B_A^- which is registered in the difference absorption spectra of native RCs at 1020 nm is absent in the analogous spectra of the mutants. The results are analyzed in terms of the participation of the B_A molecule in the primary electron transfer in the presence of a nuclear wave packet moving along the inharmonic surface of P* potential energy.

DOI: 10.1134/S000629791110004X

Key words: photosynthesis, charge separation, reaction center, wave packet, electron transfer

The reaction center (RC) of bacterial photosynthesis is a pigment–protein complex of a membrane that effectively converts light energy into the energy of separated charges as a result of series of fast electron transfer reactions. The three-dimensional structure of crystals of purple bacteria RCs from *Rhodopseudomonas* (*Blastochloris*) *viridis* and *Rhodobacter* (*Rba.*) *sphaeroides* (PDB data bank, files 1PRC and 1AIJ, consequently) is now known. *Rhodobacter sphaeroides* RC consists of three protein subunits (L, M, and H) and a number of cofactors forming two symmetry spaced branches (A and B). A primary electron donor, dimer P, consisting of two exciton-conjugated molecules of bacteriochlorophyll (BChl) P_A and P_B, is common for both branches. Each of the branches also contains monomeric BChl (B_A or B_B), bacteriopheophytin (BPheo) (H_A or H_B), and quinone (Q_A or Q_B). An atom of nonheme iron and a molecule of carotenoid are presented in the RC structure as well. In RC of purple bacteria only the A-branch is photochemically active. Primary reactions of charge separation in RCs consist of electron transfer from the lowest singlet-excited state P* to B_A within ~3 psec and further from B_A^- to H_A within ~1 psec and from H_A^- to Q_A within ~200 psec [1-5]:

$$P^* \xrightarrow{3\ \text{psec}} P^+B_A^- \xrightarrow{1\ \text{psec}} P^+H_A^- \xrightarrow{200\ \text{psec}} P^+Q_A^-.$$

Abbreviations: ΔA, absorbance change (light minus dark); BChl, bacteriochlorophyll; B_A and B_B, monomeric BChl in A- and B-branch, respectively; BPheo, bacteriopheophytin; E_m, midpoint redox potential; H_A and H_B, BPheo in A- and B-branch, respectively; P, primary electron donor, dimer BChl; P_A and P_B, BChl molecules constituting P; Q_A and Q_B, primary and secondary quinone, respectively; RC, reaction center; *Rba.*, *Rhodobacter*.

* To whom correspondence should be addressed.

Note that the $P^+B_A^-$ state is depleted several times faster than it is populated, which makes its registration much more difficult. Direct electron transfer $P^* \rightarrow P^+H_A^-$ with virtual participation of B_A levels via superexchange mechanism is possible also as well as parallel action of both types of transfer [1, 2]. At low temperatures all the mentioned reactions are accelerated 2-3-fold. The quantum yield of the charge separation process is close to unity at all temperatures [3-5].

By optical spectroscopy with femtosecond temporal resolution, oscillations were found in the kinetics of P* stimulated emission of RCs of purple bacteria [6-9]. The Fourier spectrum of these oscillations has complicated form and consists of several bands in the range of 20-400 cm^{-1}. Analogous oscillations were found in the kinetics of spontaneous fluorescence [10]. These oscillations were explained by nuclear wave-packet motion along the potential energy surface of P* [7, 8, 11]. Similar oscillations were revealed in the kinetics of charge separated states $P^+B_A^-$ and $P^+H_A^-$ by studying the absorption band of B_A^- at 1020 nm and the absorption band of H_A at 760 nm [12-17]. Oscillations in the kinetics of P* stimulated emission at 945 nm and of B_A^- absorption at 1028 nm were found in *Chloroflexus aurantiacus* RCs at 90 K [18]. Identification of the bands from Fourier spectra of the oscillations is quite difficult. The main band of the oscillations of P* emission at 940 nm and of B_A^- absorption at 1020 nm is at ~130 cm^{-1} and reflects, most probably, vibration motion inside the dimer P [16]. This is indicated by a presence of the similar mode at 140-150 cm^{-1} in the oscillations of P* emission of YM210L and YM210W mutants, in which charge separation is practically absent during several psec after excitation [18]. A strong mode at 32 cm^{-1}, which may reflects a rotation of crystallographic water HOH55 in the RC structure, is also represented in the oscillations of the B_A^- band at 1020 nm [16]. Note that the oscillations at ~130 cm^{-1} in the kinetics of B_A^- absorption are in phase with the analogous oscillations in the kinetics of P* stimulated emission at 940 nm and in anti-phase with these oscillations at 900 nm [13]. It was found by molecular dynamic methods that motions of the protein surrounding P and B_A molecules modulate the position and orientation of these molecules at frequencies in the range of 10-100 cm^{-1} [19]. There are two groups in each of two BChl molecules from the dimer P that are able to accept a proton during formation of hydrogen bonds. These are the 9-keto group of ring V and the 2-acetyl group of ring I. A full set of point mutant RCs is available in which new hydrogen bonds are created or already existing hydrogen bonds are broken in the dimer P [20-24]. In native *Rba. sphaeroides* RCs there is only one hydrogen bond between HisL168 and the 2-acetyl group of ring I in P_L. This bond is absent in the HL168F mutant, in which His is replaced by Phe. An additional hydrogen bond with the 2-acetyl group of ring I in P_M is created by the opposite replacement of Phe by His in the FM197H mutant. Replacement of Leu by His in the LL131H mutant creates an additional hydrogen bond with the 9-keto group of ring V in P_L. Analogous replacement of Leu by His in the LL160H mutant creates a hydrogen bond with the 9-keto group of ring V in P_M. Addition or removal of hydrogen bonds is determined by spectroscopy decrease or increase of characteristic vibration frequencies of corresponding groups. Combining the mentioned mutations, it is possible to create double or triple mutants with two or three additional hydrogen bonds in RCs [21, 22]. Removal of a hydrogen bond in the HL168F mutant decreases the midpoint redox potential E_m of the P/P^+ pair by 95 mV in comparison with native RCs. On the contrary, creation of new hydrogen bonds increases E_m by 60-125 mV depending of the specific mutation. This effect is additive in the complex mutants, which allows varying E_m over the wide range from −95 to 260 mV with respect to $E_m \approx 505$ mV in native *Rba. sphaeroides* RCs [21, 22]. Increasing E_m means an increase of energy levels of charge separated states $P^+B_A^-$, $P^+H_A^-$, and $P^+Q_A^-$, that leads to slowing of the primary reactions of charge separation and to accelerating of recombination $P^+Q_A^- \rightarrow PQ_A$ if the P* level is unchanged. In the present work, coherent phenomena accompanying charge separation were studied in mutant LL131H and LL131H/LM160H/FM197H *Rba. sphaeroides* RCs at 90 K. As a result of adding of three hydrogen bonds, in the triple mutant the E_m value is increased by 260 mV in comparison with native RCs. Estimations show that in native *Rba. sphaeroides* RCs the $P^+B_A^-$ level is lower than the P* level by 40-70 mV [25] and the $P^+H_A^-$ level is lower than the P* level by 120-200 mV [1, 2]. This means that a situation is possible when both levels are higher than P* in the LL131H/LM160H/FM197H mutant, which blocks the process of charge separation and conserves the P* state on the picosecond time scale. In this case the influence of charge separation on coherent phenomena is absent in the P* stimulated emission band that makes its analysis easier. In the LL131H mutant the E_m value is increased by 80 mV in comparison with native RCs. Raising of the $P^+B_A^-$ level by this value puts it close to the level of P*, and raising of the $P^+H_A^-$ level by the analogous value keeps this level lower than the level of P*. In this case influence of charge separation on the coherent phenomena in the P* band should be weaker in the LL131H mutant in comparison with native RCs.

MATERIALS AND METHODS

Genetic manipulations and obtaining of mutant RCs were carried out according to [21, 22]. Mutant RCs, as well as native *Rba. sphaeroides* RCs, were isolated by treatment of membranes with LDAO followed by chromatography with DEAE cellulose [26]. The RCs were suspended in 10 mM Tris-HCl (pH 8.0)/0.1% Triton X-

100 buffer (TT buffer). Low temperature measurements at 90 K were performed on samples containing 65% glycerol. The optical density of the samples was 0.5 at 860 nm at room temperature. To keep the state $PB_AH_AQ_A^-$, 5 mM sodium dithionite was added to the RC samples.

Measurements of absorption differences (light – dark) with femtosecond resolution were performed with a laser spectrometer consisting of a Tsunami Ti-sapphire laser with mode locking (Spectra Physics, USA). Laser pulses were amplified in a multi-passed Ti-sapphire amplifier and were used for generation of probing continuum in a mixture of ordinary and heavy water (1 : 1). Part of the continuum of ~40 nm width centered at 880 nm was used for excitation. A polychromator and optical multichannel analyzer (Oriel, France) were used for difference absorption spectra registration. Measuring frequency of the spectrometer was 15 Hz. Durations of pump and probe pulses were 18 fsec. Delays between pump and probe pulses were set with 0.1 fsec accuracy. Residual dispersion in the range of 940-1060 nm was less than 25 fsec.

Difference absorption spectra measured at various delays in the range of 0-4 psec with 30 fsec step were the primary data. Each spectrum was a result of averaging over 3000-8000 measurements. The error of absorption measurements was $(1\text{-}3)\cdot10^{-5}$ OD. Amplitudes of spectral bands were measured at their maximums at various delays. The kinetics of absorption changes (ΔA) were plotted for different wavelengths using the measured amplitudes of absorption or bleaching bands. Oscillatory components of the kinetics were found by subtraction of polynomial approximated curves from the experimental kinetics. The oscillations were further Fourier-analyzed for obtaining their frequency spectra.

RESULTS

In Fig. 1, difference (light – dark) absorption spectra of RCs from LL131H and LL131H/LM160H/FM197H *Rba. sphaeroides* mutants measured at 90 K are shown together with analogous spectra for native *Rba.*

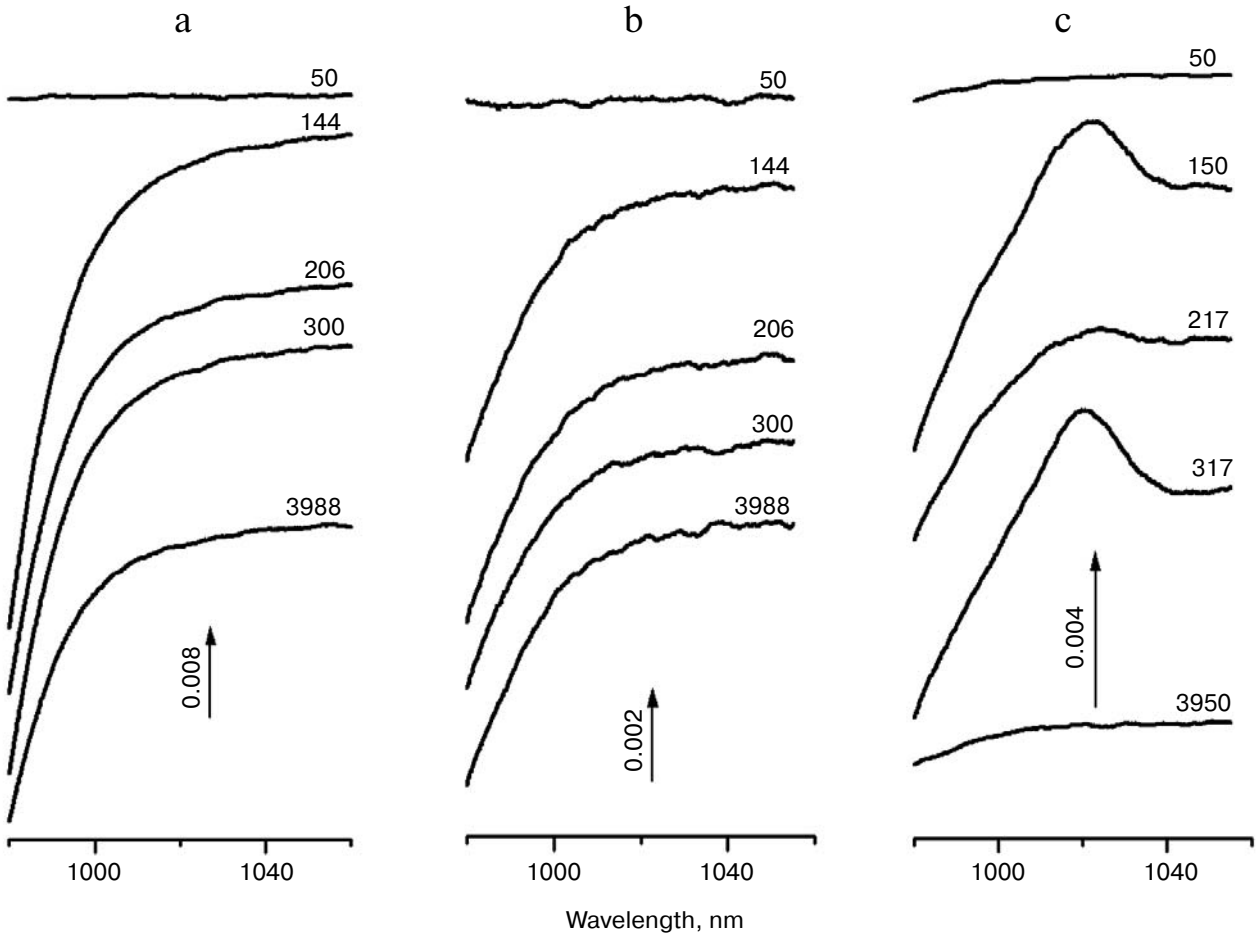

Fig. 1. Difference (light – dark) absorption spectra of mutant LL131H (a), mutant LL131H/LM160H/FM197H (b), and native (c) RCs of *Rba. sphaeroides* in the 980-1060 nm range at 90 K. The RCs were excited by 18-fsec pulses at 870 nm. Delays with respect to excitation moment are given by numbers in fsec. Spectra are vertically shifted for clearness.

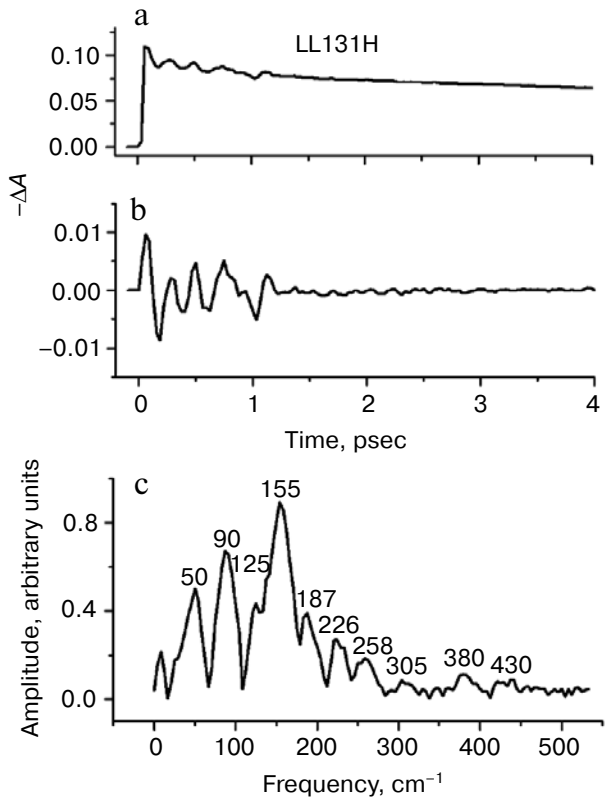

Fig. 2. Kinetics ΔA (a), oscillatory component of these kinetics (b), and Fourier spectrum of oscillatory component (c) of mutant LL131H *Rba. sphaeroides* RCs at 950 nm (P* stimulated emission band). The RCs were excited by 18-fsec pulses at 870 nm at 90 K. Numbers in Fig. 2c are frequencies of band maxima in cm^{-1}.

sphaeroides RCs in the 980-1060 nm range for several fsec delays. In native RCs a weak absorption band of anion B_A^- is observed in the area of 1020 nm, which repeats results obtained earlier [16]. The amplitude of this band changes in an oscillatory manner when varying the delay, but its form and spectral position remains unchanged. This band is not detected in the spectra of either mutant, which can indicate a nonparticipation of the B_A molecule in primary charge separation. At wavelengths less than 995 nm, a bleaching caused by P* stimulated emission dominates in the RC spectra. A variety of difference spectra measured with 30 fsec delay step was used for plotting the kinetics of P* emission shown in Figs. 2-4.

The kinetics of P* stimulated emission of the LL131H mutant are approximated satisfactorily by a sum of two exponentials with time constants 16 psec (82%) and 0.5 psec (16%) (Fig. 2). The presence of several components in the kinetics of P* stimulated emission of this mutant was noted in [24] also. The time constant of the main component (16 psec) exceeds the analogous time for native RCs (~1.3 psec; Fig. 4) by more than 10-fold, which indicates a marked change in the energetics of the LL131H mutant. The presence of much faster component (0.5 psec) can be a consequence of back reaction $P^+B_A^- \rightarrow P^*$ (see "Discussion"). Oscillations with complicated form decaying almost completely during 1.2 psec after excitation are seen in the P* kinetics of the LL131H mutant (Fig. 2b). The amplitude of these oscillations does not exceed 10% of the average level of the non-oscillating part of the kinetics. The main part of the oscillations has the shape of five peaks separated by ~220 fsec period. Note that the amplitude of these peaks does not decrease monotonously with time as takes place during an ordinary attenuation of oscillations. On the contrary, the amplitude of the third peak is bigger than that of the second, and the amplitude of the fourth peak is comparable with the amplitude of the third peak. This picture may be a consequence of strong low-frequency modulation of the kinetics. Indeed, a Fourier spectrum of the oscillations of the LL131H mutant contains a set of bands in the range of 20-450 cm^{-1}, and also the spectrum amplitude of the lowest frequency mode at 50 cm^{-1} is almost the same as the amplitude of the cen-

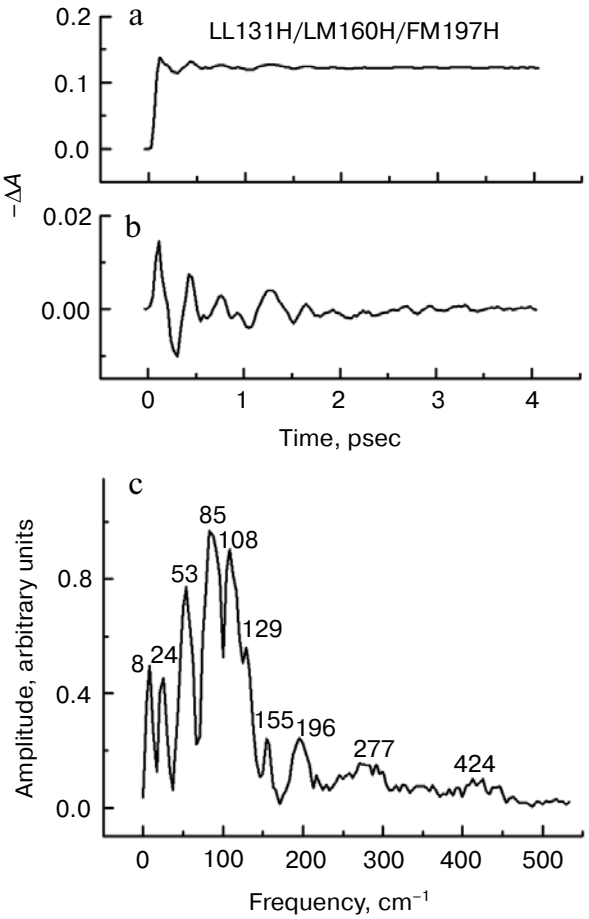

Fig. 3. Kinetics ΔA (a), oscillatory component of these kinetics (b), and Fourier spectrum of oscillatory component (c) of mutant LL131H/LM160H/FM197H *Rba. sphaeroides* RCs at 940 nm (P* stimulated emission band). The RCs were excited by 18-fsec pulses at 870 nm at 90 K. Numbers in Fig. 3c are frequencies of band maxima in cm^{-1}.

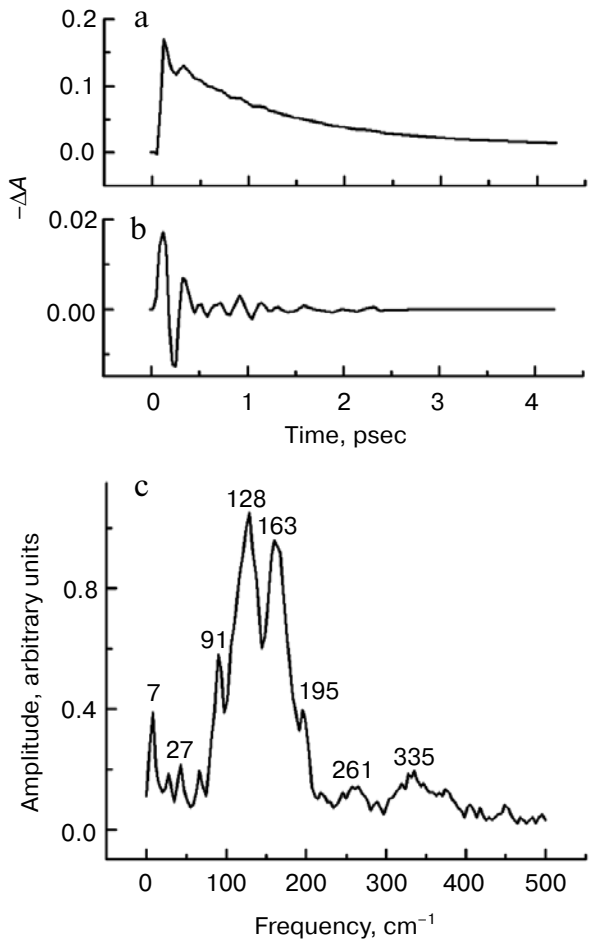

Fig. 4. Kinetics ΔA (a), oscillatory component of these kinetics (b), and Fourier spectrum of oscillatory component (c) of native *Rba. sphaeroides* RCs at 940 nm (P* stimulated emission band). The RCs were excited by 18-fsec pulses at 870 nm at 90 K. Numbers in Fig. 4c are frequencies of band maxima in cm^{-1}.

tral mode at 155 cm^{-1} (Fig. 2c). Most of the modes have a bandwidth of ~20-30 cm^{-1} and are separated by an interval of 30-40 cm^{-1}. Noted peculiarities are characteristic for the oscillations in the P* kinetics of native RCs also (Fig. 4). The amplitude of the fifth oscillation peak is bigger than of the almost same amplitude third and fourth peaks in these RCs (Fig. 4b), and the Fourier spectrum of the oscillations contains bands separated by the interval of ~30 cm^{-1} (Fig. 4c). Unlike in the LL131H mutant, the Fourier spectrum of the oscillations in native RCs does not have strong low-frequency bands around ~50 cm^{-1}.

The P* stimulated emission of the LL131H/LM160H/FM197H mutant shows almost no decay during first 4 psec after excitation (Fig. 3). Measurements of the P* kinetics in the delay range of 0-2 nsec gave 276-psec value of the time constant of the main component of the decay, which is close to the value of 290 psec obtained at 20 K in [22]. This value is close to the recombination time of P* → P that is estimated as 300 psec [1, 2], which indicates a significant part of the recombination in the P* kinetics. Nevertheless, charge separation is observed in this triple mutant at 20 K with the formation of the $P^+H_A^-$ and $P^+Q_A^-$ states with low quantum yield [22]. Thus, the oscillations in the P* kinetics (Fig. 3b) existing during ~2 psec after excitation reflect mostly the state of excited dimer P and is not connected with charge separation. Seven main peaks separated by ~250-fsec period can be seen in these oscillations. Very weak oscillations with the same period are seen at delays >2 psec, which distinguishes the triple mutant from the LL131H mutant (Fig. 2b). The amplitude of the first peak reaches ~10% of the ΔA value. Note that the amplitude of the fifth peak is bigger than of the preceding third and fourth peaks, and the amplitude of the sixth peak is comparable with the amplitude of the fourth peak (Fig. 3b). Similar irregularity is seen in the kinetics of the LL131H mutant (Fig. 2b) and in the kinetics of native RCs (Fig. 4b). The presence of a large amount of the weakly attenuated oscillation peaks in the P* kinetics makes this triple mutant similar with the YM210W and YM210L *Rba. sphaeroides* mutants in which primary charge separation is strongly slowed because of the absence of tyrosine M210 [18]. The Fourier spectrum of the oscillations of the triple mutant contains a variety of bands in the range of 20-450 cm^{-1} (Fig. 3c). The modes at 85 and 108 cm^{-1} dominate among them, and low-frequency modes with marked amplitude are seen at 24 and 53 cm^{-1}. The frequency interval between most of the neighboring modes is ~30-40 cm^{-1} with bandwidth of ~20-30 cm^{-1}, as it is in the LL131H mutant. Unlike in native RCs and in the LL131H mutant RCs, the P* oscillations have lower central frequency in the triple mutant RCs. An analogous frequency shift is observed in oscillations of the FM197H mutant [24] and of the YM210L/FM197Y double mutant [27].

DISCUSSION

In Fig. 5 a scheme of mutual arrangement of energy levels of the P*, $P^+B_A^-$, and $P^+H_A^-$ states is shown for native and mutant *Rba. sphaeroides* RCs. Successive electron transfer takes place in native RCs from P* to B_A and from B_A^- to H_A with very small activation energy of both reactions $E_a = \lambda/4(1 + \Delta G/\lambda)^2$, where λ is reorganization energy and ΔG is free energy of reaction. In Fig. 5, ΔG value is equal to the energy difference between the bottoms of the potential curves. In native RCs, this difference is estimated as 350-550 cm^{-1} between P* and $P^+B_A^-$ levels [25] and as 1300-2000 cm^{-1} between P* and $P^+H_A^-$ levels [2]. Reaction rates K_{12} and K_{23} can be estimated by the formula of Hopfield [28]:

$$K = (2\pi/\hbar)V^2(4\pi\lambda\varepsilon)^{-0.5}\exp(-E_a/\varepsilon), \quad (1)$$

where ħ is the Plank constant, V is matrix element of electron conjugation, $\varepsilon = (\hbar\omega/2)\coth(\hbar\omega/2K_BT)$ is average energy of oscillator, ω is characteristic frequency of intramolecular or intermolecular oscillations, K_B is Boltzmann constant, and T is temperature. In high temperature limit at $\hbar\omega << K_BT$ we have $\varepsilon = K_BT$ and formula (1) is transformed to the well-known Marcus formula [29]. With λ_{12} = 800 cm^{-1}, ΔG_{12} = –450 cm^{-1}, λ_{23} = 1000 cm^{-1}, ΔG_{23} = –1000 cm^{-1}, ω = 1000 cm^{-1}, V_{12} = 30 cm^{-1}, V_{23} = 50 cm^{-1}, T = 90 K we obtain K_{12} = 1/(1.4 psec) and K_{23} = 1/(0.4 psec) in native RCs, which is close to the experimental data [16]. The transfer rate from B_A^- to H_A is 3.5 times greater than transfer rate from P* to B_A. An estimation of direct electron transfer rate from P* to H_A by superexchange mechanism [30] with λ_{13} = 1500 cm^{-1} gives the much smaller value of K_{13} ~1/(300 psec).

In the LL131H mutant, the $P^+B_A^-$ and $P^+H_A^-$ levels are raised with respect to P* level by ~640 cm^{-1} (80 mV) (Fig. 5) [20]. The $P^+B_A^-$ level becomes higher than the P* level by 190 cm^{-1} in this case, which leads to decreasing of K_{12} rate and to appearance of backward reaction $P^+B_A^- \rightarrow$ P* with the rate $K_{21} = K_{12}\exp(\Delta G_{12}/\varepsilon)$ exceeding the rate of forward reaction K_{12}. In this case the population of the $P^+B_A^-$ state becomes so small that it cannot be found experimentally. Nevertheless, the presence of the fast component with time constant ~$1/K_{23}$ = 0.5 psec in the P* kinetics, which can appear only due to the back reaction $P^+B_A^- \rightarrow$ P* (Fig. 2), indicates the participation of B_A in electron transfer. Indeed, the solution of a system of rate equations including the back reaction K_{21} for the LL131H mutant shows that the P* kinetics is a sum of two exponentials with the following constants:

$$\alpha_1 = (K_{12} + K_{21} + K_{23})/2 + \\ + ((K_{12} + K_{21} + K_{23})^2/4 - K_{12}K_{23})^{0.5};$$

$$\alpha_2 = (K_{12} + K_{21} + K_{23})/2 - \\ - ((K_{12} + K_{21} + K_{23})^2/4 - K_{12}K_{23})^{0.5}. \quad (2)$$

With $K_{23} >> K_{12}$, K_{21} we have $\alpha_1 \sim K_{23}$, $\alpha_2 \sim K_{12}$. Estimations by formula (1) give the following values of reaction rates: K_{12} = 1/(12.5 psec), K_{21} = 1/(2.6 psec). With unaltered rate K_{23} = 1/(0.4 psec) we have α_1 = 1/(0.36 psec) and α_2 = 1(14.5 psec), which is close to the experimental values of these constants 1/(0.5 psec) and 1/(16 psec), respectively. An estimation of superexchange rate in the LL131H mutant gives a value K_{13} ~ 1(500 psec), which is much less than the rates of "ordinary" electron transfer [30]. Thus, the LL131H mutant demonstrates two-step electron transfer in spite of unfavorable position of the $P^+B_A^-$ level higher than P* level and impossibility of direct detection of the $P^+B_A^-$ state in this experiment.

In the LL131H/LM160H/FM197H triple mutant, the $P^+B_A^-$ and $P^+H_A^-$ levels are raised with respect to P* by ~2080 cm^{-1} (260 mV) (Fig. 5). In this case the $P^+B_A^-$ level becomes higher than P* by 1630 cm^{-1}, and the $P^+H_A^-$ level becomes higher than P* by 630 cm^{-1}, which undoubtedly blockades the two-step mechanism. Nevertheless, electron transfer to Q_A is detected in this mutant even at 20 K with very small quantum yield ~10% [22]. One cannot reveal the spectrally pure $P^+H_A^-$ state in this case, which may means the presence of several close $P^+H_A^-$ states in the same RC or the presence of several types of RC with different $P^+H_A^-$ states (heterogeneity). An estimation of superexchange rate in the triple mutant gives a value K_{13} ~ 1(5 nsec) with the rate of backward superexchange $K_{31} \geqslant K_{13}$ [30]. A solution of the rate equation system for this mutant shows that an exponential with the rate constant $K_0 + K_{13}$ dominates in the P* kinetics, where K_0 is relaxation rate of the P* state. Taking K_0 ~ 1/(300 psec) [1, 2], we obtain $K_0 + K_{13}$ ~ 1/(280 psec), which is close to the experimental value 276 psec. Note that at T = 300 K a decay of the P* kinetics with 50-psec time constant is detected in this triple mutant, while the quantum yield of charge separation reaches 50% [22]. This indicates the possible presence of thermal activation of the two-step mechanism of charge separation. Formula (2) gives a value α_2 = 1/(50 psec) for K_{12} = 1/(38 psec) that corresponds to the value ΔG_{12} = 700 cm^{-1} rather than 1630 cm^{-1}. This may means that dynamic decrease of the $P^+B_A^-$ level takes place on the picosecond time scale. One of possible mechanisms of this decrease is a reorientation of the OH group in tyrosine M210 due to charges appearing on P^+ and B_A^- [16].

The presence of a large number of spectral components, the origin of which remains not quite clear, is a characteristic feature of the Fourier spectra of the oscillations in the P* stimulated emission kinetics of native and mutant RCs (Figs. 2-4 and [5-9, 12-18, 27]). A similar feature is noted in the kinetics of charge separated states as well. A hypothesis was advanced in [16] that some of these spectral components may reflect rotation of the HOH55 molecule with fundamental frequency of 32 cm^{-1}, overtones of which with numbers up to seven are detected especially clearly in the $P^+B_A^-$ state kinetics in pheophytin-modified RCs. An attempt for an alternative explanation of these features is made below.

First of all, the hypothetical possibility of parametric modulation of rate constants of forward and backward reactions is examined for the simplest scheme of charge separation P* ↔ P^+A^-. The nature of this external modulation may consist in a motion of the protein environment of chromatophores. The rate constant of forward reaction K_{12} was determined by formula (1), and the backward reaction had rate constant $K_{21} = K_{12}\exp(\Delta G/\varepsilon)$. The two following mechanisms of parametric modulation

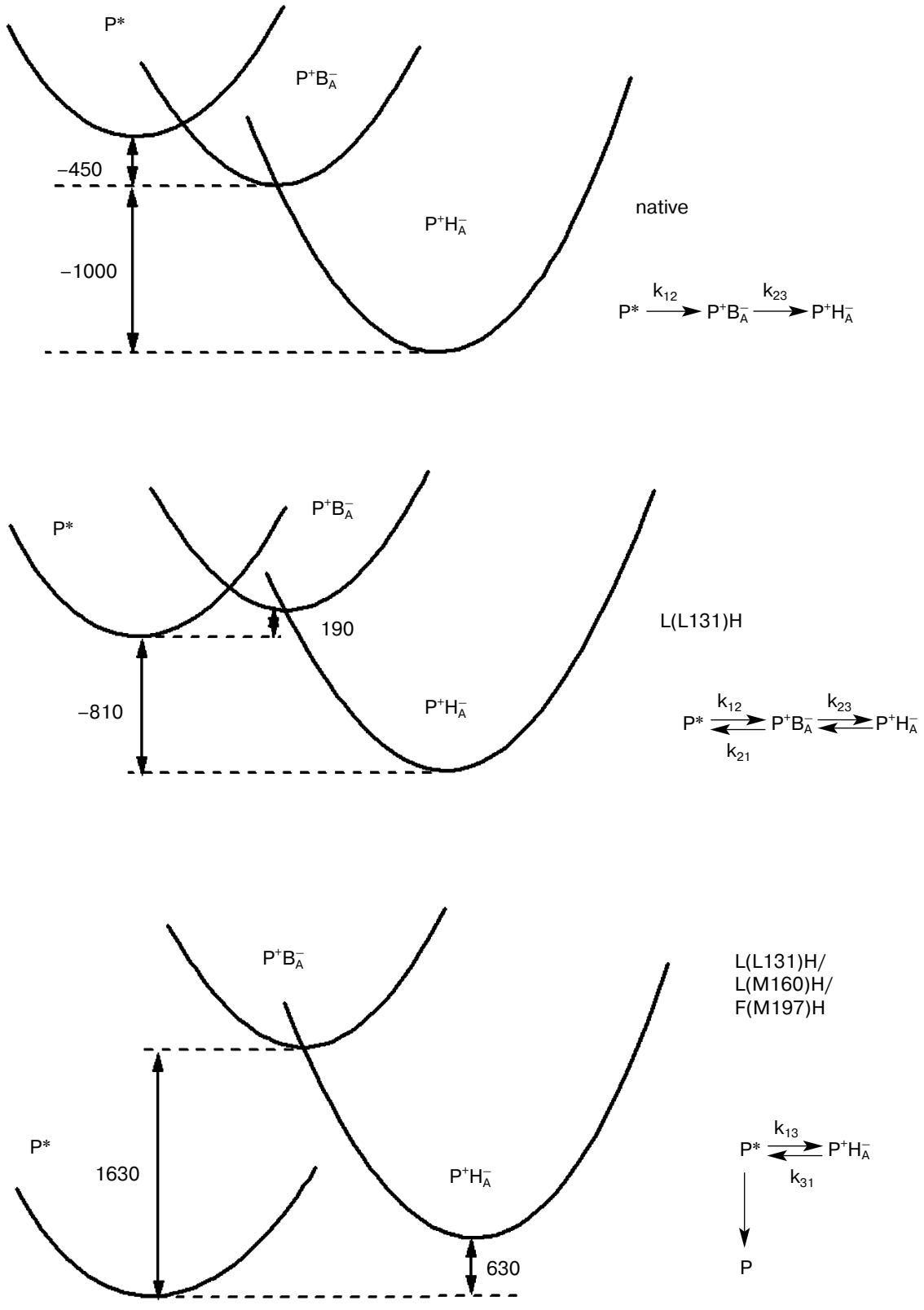

Fig. 5. Schematic arrangement of energy levels of P*, $P^+B_A^-$, and $P^+H_A^-$ states for native (top figure) and mutant (LL131H – middle figure, LL131H/LM160H/FM197H – bottom figure) *Rba. sphaeroides* RCs. Energy differences are given by numbers in cm^{-1}. Schemes of primary reactions of charge separation are shown on the right.

were examined: 1) modulation of energy level difference ΔG; 2) modulation of distance R between donor and acceptor molecules. The first case corresponds to vertical shift of potential energy surfaces of P* and P^+A^- states with respect to each other (see Fig. 5) with unaltered R. The second case corresponds to horizontal shift of these surfaces with unaltered value ΔG. In the second case the modulation of R leads to the modulation of both electron conjugation $V \sim \exp(-aR)$, where $a \approx 0.14$ nm^{-1} for the protein [31], and the reorganization energy $\lambda = m\omega^2R^2/2$. Harmonic and non-damped modulation with two independent frequencies was studied. A system of rate equations (3) was solved numerically:

$$dP/dt = -K_{12}P + K_{21}A,$$

$$dA/dt = -K_{21}A + K_{12}P. \quad (3)$$

Here P and A are populations of the P* and P^+A^- states, $P + A = \text{const}$, and K_{12} and K_{21} are functions of time. Parametric modulation leads to appearance of oscillations in the kinetics of the P* and P^+A^- states with opposite phases due to closeness of the system. Results of Fourier analysis of the oscillations for the P* state are shown in Fig. 6. Both types of modulations lead to a similar result: harmonics and sum-difference frequencies appear in the oscillation spectrum together with preset frequencies of external modulation ω1 and ω2. A reason of the appearance of new frequencies is the nonlinear dependence of the rate constants K_{12} and K_{21} on varied values ΔG and R. The spectral amplitude of all new bands is much less than those of the ω1 and ω2 bands except for the lowest band ω1−ω2. This result is a consequence of the fact that P and A values are proportional to $\int K_{12}dt$ and $\int K_{21}dt$ leading to an effect of demodulation that is a suppression of high frequency components and increasing of low frequency components in the oscillation spectra. Weak bands in the oscillation spectra being observed experimentally in the area of 200-450 cm^{-1} may be harmonics of more intense bands at 100-150 cm^{-1} (Figs. 2-4). On the whole, the oscillation spectra shown in Fig. 6 are far from the experimental ones, which compels us to search for new mechanisms explaining the appearance of the large number of bands in the oscillation spectra.

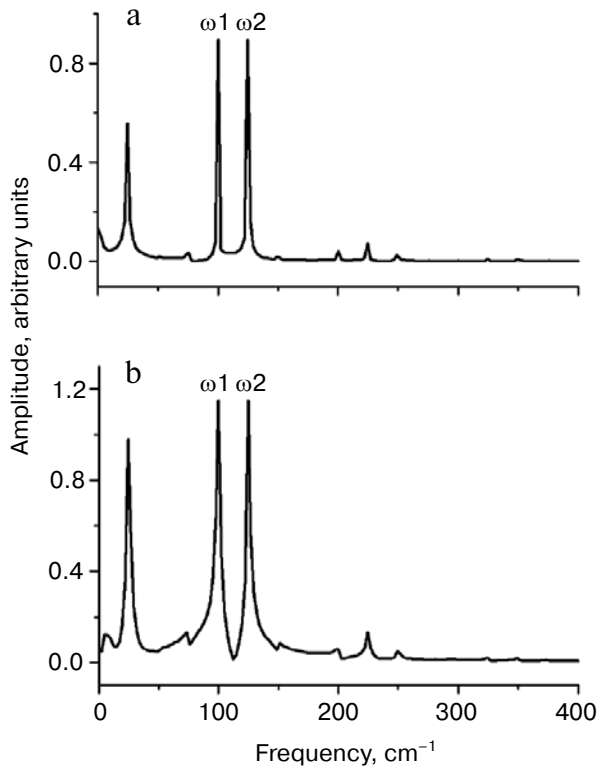

Fig. 6. Calculated Fourier spectra of P* stimulated emission oscillations caused by harmonic parametric modulation of rate constants of forward and backward reactions P* ↔ P^+A^- at two frequencies ω_1 and ω_2. a) Modulation of energy level difference ΔG; b) modulation of distance R between donor and acceptor molecules. See details in the text.

One possible explanation for the variety modes detected in the oscillation spectra is inharmonicity of P* potential energy surface on which a wave-packet moves. Let us consider a simplest case of one-dimension motion along the x-axis. The wave-packet is a superposition of wave-functions of vibrational sublevels which are excited by the light pulse:

$$\Psi(x, t) = \sum_n C_n \exp(-i\omega_n t)\, \Psi_n(x), \quad (4)$$

where $\omega_n = E_n/\hbar$, E_n are eigenvalues of sublevel energy, C_n are coefficients. The motion of the wave-packet as a whole is described by temporal dependence of its center of gravity:

$$\langle x \rangle = \int \Psi^*(x,t) x \Psi(x,t) dx, \quad (5)$$

where integration is over infinite terms [32]. Taking into account the orthogonality of the wave functions $\Psi_n(x)$ and using Eq. (4), we have the following expression for $\langle x \rangle$:

$$\langle x \rangle = \sum_n C_{n+1} C_n \times$$

$$\times \cos((\omega_{n+1} - \omega_n)t) \int \Psi_{n+1}(x) x\, \Psi_n(x) dx. \quad (6)$$

For harmonic potential all vibrational sublevels are equidistant, which leads to wave-packet motion by the simple harmonic law:

$$\langle x \rangle = \cos(\omega t) \sum_n C_{n+1} C_n \int \Psi_{n+1}(x) x\, \Psi_n(x) dx. \quad (7)$$

Thus, the wave-packet gravity center performs a complicated motion, which is a sum of harmonic oscillations of different amplitudes with difference frequencies.

This motion can be considered as a superposition of harmonic motions of separate parts of the wave-packet with frequencies $\omega_{n+1}-\omega_n$. In fact, the value $<x>$ contains all information about the vibrational spectrum of the P* excited state. The oscillations in the P* kinetics at fixed wavelength are visualized in this motion and, therefore, should have the same spectra as $<x>$. Note that the dependence $<x>(t)$ does not describe fine coherent effects connected with a change of wave-packet form. Inharmonicity of the potential leads to nonlinear dependence of energy E_n on sublevel number n:

$$E_n/\hbar\omega = (n + 1/2) - \alpha(n + 1/2)^2 + \\ + \beta(n + 1/2)^3 - \gamma(n + 1/2)^4 + ..., \quad (8)$$

where α, β, γ ... – parameters of inharmonicity [33]. The real potential can have very complicated dependence on space coordinates, so the series (8) at fixed parameters of inharmonicity approximates satisfactorily only some of the energy levels. The total number of the energy levels given by (8) can be both finite in the case of its condensation with increase of n and infinite in the case of its rarefaction with increase of n.

The number of excited vibrational sublevels also depends on the bandwidth of the excitation pulse and on the space overlapping of the wave-functions $\Psi_n(x)$ with the ground state wavefunction of the non-excited P state. A light pulse of 20-fsec duration with 870-nm central wavelength has bandwidth ~40 nm (530 cm^{-1}) at half-maximum and ~80 nm (1060 cm^{-1}) at the basis. The number of excited sublevels N can be ~8 when the average distance between the sublevels is $\hbar\omega$ ~ 130 cm^{-1}, and about half of them can considerably contribute to $<x>$ in this case. Taking into account that the wavelength of 0–0 transition in dimer P of *Rba. sphaeroides* is 907 nm [34], we obtain the sublevel number N_{max} ~ 4 corresponding to excitation maximum at 870 nm. Space shift of the P* potential energy surface with respect to those of P should leads to the shift of maximal overlapping of the wave-functions of the ground and excited P states to higher n. Unfortunately, sufficient information about this shift and the potential profiles of the P and P* states is absent. It is clear that if the P potential is spaced narrower than the P* potential and the shift of the P* surface with respect to the P surface is sufficient, then the number of excited sublevels should not be large and the number of sublevels excited maximally should be well above 0. So, the estimation of the number of the excited sublevels N ~ 8 is the upper one and can be decreased by taking into account the space factor.

In Fig. 7, results of a calculation of the $<x>$ value dependence on time and Fourier spectrum of this dependence are presented for different sets of inharmonicity parameters. Inharmonicity constants and constant coefficients determining relative contribution of different spectral components to $<x>$ were selected on the base of the best coincidence of the calculated Fourier spectra of the P* stimulated emission oscillations in the LL131H/LM160H/FM197H *Rba. sphaeroides* triple mutant with the experimental ones. As shown above, charge separation is slowed in this mutant so that the P* kinetics reflects a condition of dimer P itself during several tens of picoseconds after excitation. In the case of non-coincidence of some calculated mode frequency with any of the experimental mode frequencies, spectral amplitude of the nearest experimental mode was used as the amplitude of this calculated mode. Processes of different nature of non-reversible dissipation of the wave-packet were modeled by exponential decay according to [35]. The decay constant was taken as 2 psec. It was assumed in the calculations that at $t = 0$ the wave-packet appears on the left short-wavelength side of the P* potential curve. The wave-packet appears on the right long-wavelength side of this curve after a delay of approximately half of the main period of the oscillations, that is ~120 fsec. Effects connected with residual dispersion of excitation pulse leading to excitation of different vibrational sublevels not at the same time were not examined. Initial spreading of the wave-packet when it appears on the P* long-wavelength slope the first time was not taken into account. Thus, the wave-packet dynamics on the P* long-wavelength slope corresponding to 940-nm emission was described by expression (6) with $\sin((\omega_{n+1} - \omega_n)t)$ instead of $\cos((\omega_{n+1} - \omega_n)t)$.

When only one inharmonicity parameter α is taken into account in the E_n expansion, the wave-packet decays and then is restored periodically (Fig. 7a). This process is fully reversible and continues for an unlimited time if damping is absent. The number of excited energy sublevels is limited in this case: the energy sublevels are concentrated with n and a difference $E_{n+1} - E_n$ becomes equal to 0 at $n = 8$. As directly follows from (8), the difference $E_{n+1} - E_n$ linearly depends on n, while the distance between modes in the Fourier spectrum of the $<x>(t)$ dependence is constant and equal to 2α. The Fourier spectrum mode with maximal frequency is formed from the two lowest energy sublevels with numbers 0 and 1, and the lowest frequency mode is build from the two highest sublevels with numbers 7 and 8. The main period approximately corresponding to the component with maximal amplitude can be seen in the $<x>$ oscillations in spite of the presence of several spectral components. Wave-packet decay can take place during one oscillation period, while the revival comes after several periods (Fig. 7a). The wave-packet decay cannot be complete: the oscillations with small amplitude are always remained after disappearance of the main peak. The wave-packet revival can be partial or complete: usually, one complete revival is after several partial revivals. The decay time and revival period are increased with decreasing inharmonicity. These peculiarities are completely confirmed by a more

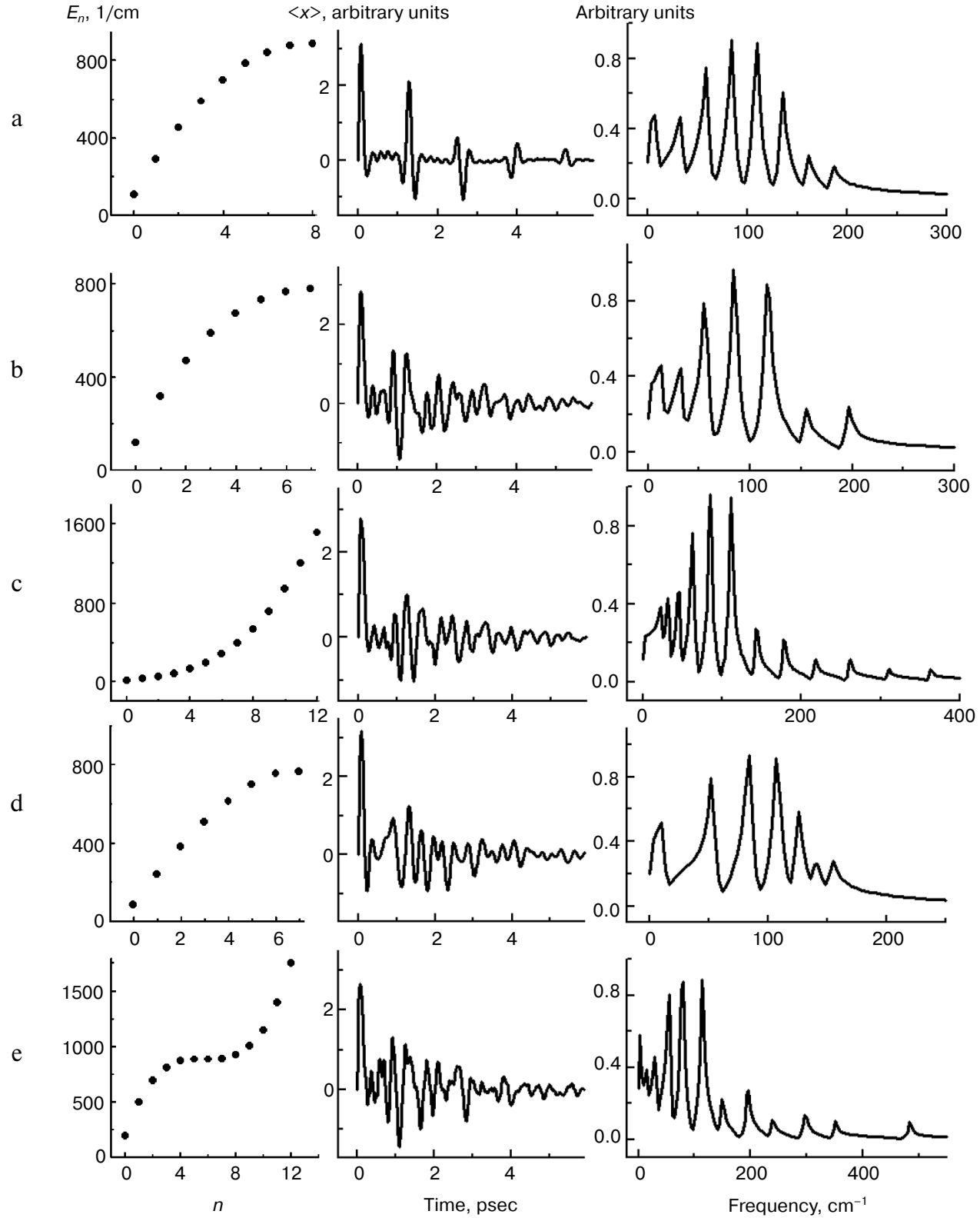

Fig. 7. Calculated dependences of energy E_n of vibrational sublevels on their numbers n (left column), dependences of wave-packet gravity center on time $\langle x \rangle(t)$ (middle column), and Fourier spectra of the $\langle x \rangle(t)$ dependences (right column) for various sets of inharmonicity parameters of potential energy surface of P* state. a) $\hbar\omega = 212.8$ cm^{-1}, $\alpha = 0.06$; b) $\hbar\omega = 244.7$ cm^{-1}, $\alpha = 0.1$, $\beta = 0.0031$; c) $\hbar\omega = 18.6$ cm^{-1}, $\alpha = 0.06$, $\beta = 0.04$; d) $\hbar\omega = 170.2$ cm^{-1}, $\alpha = 0.05$, $\beta = 0.001$, $\gamma = 0.0006$; e) $\hbar\omega = 425.6$ cm^{-1}, $\alpha = 0.16$, $\beta = 0.0085$. See details in the text.

rigorous and consistent theoretical approach of the wave-packet dynamics in inharmonic potentials [36]. It is interesting that exact solution of the Schrodinger equation with Morse potential $U = D(1-\exp(-aR))^2$, where D is dissociation energy, a is a parameter defining a characteristic well width, R is distance, corresponded to one α parameter inharmonicity. According to quantum-mechanical calculations, the energy of vibrational sublevels is equal within the accuracy of ~$\hbar^2$:

$$E_n = \hbar\omega\,(n + 1/2) + 3/2(n^2 + n +$$

$$+ 1/2)\hbar^2((1/4!)d^4U(R = 0)/dR^4)/(m^2\omega^2) -$$

$$- 15/4(n^2 + n + 11/30)\hbar^2((1/3!)d^3U(R = 0)/$$

$$/dR^3)/(m^3\omega^4), \quad (9)$$

where m is effective mass, ω is fundamental frequency closed to the maximal frequency of the oscillation spectrum [32]. It is follows from this expression that for Morse potential the distance between the Fourier spectrum modes of the $<x>(t)$ dependence is equal:

$$2\alpha = 2Da^4\,\hbar^2/(m^2\omega^2). \quad (10)$$

Taking into account that for Morse potential $Da^2 = m\omega^2/2$, we obtain the final expression for the distance between modes:

$$2\alpha = \hbar^2\,\omega^2/2D. \quad (11)$$

For $\hbar\omega = 250$ cm^{-1} and D ~ 1000 cm^{-1} we have the value 2α ~ 30 cm^{-1} that is closed to the experimental value. For evaluation of mass m let us use the fact that the decrease of the central oscillation frequency from 150 to 100 cm^{-1} takes place in the P* emission band of the YM210L/FM197Y *Rba. sphaeroides* mutant as a result of adding of a tyrosine residue to dimer P [27]. Supposed that in the simplest case these oscillations reflect elastic vibration of dimer P fragments along a single axis, we have the following expression for the vibration frequencies:

$$\omega_1 = (\kappa/m)^{0.5} = 150\ \text{cm}^{-1},$$

$$\omega_2 = (\kappa/(m + m_{tyr}))^{0.5} = 100\ \text{cm}^{-1}, \quad (12)$$

where k is coefficient of elasticity, $m_{tyr} = 163$ Da is tyrosine mass. As a result the expression for m has the form:

$$m = m_{tyr}\,\omega_2^2/(\omega_1^2 - \omega_2^2), \quad (13)$$

whence we have m = 130.4 Da. Note that a fragment of the tetrapyrrole ring of P_A or P_B can have this mass. Using a connection of parameters $Da^2 = m\omega^2/2$ for Morse potential, we obtain an evaluation for a: $a = 0.17$ nm^{-1}.

Repeated decay and revival of wave-packets is clearly detected in the experiments of coherent femtosecond photo-dissociation of rare vapors of simple compounds like I_2 or ICN (review see in [37]). For condensed media this effect is not typical probably because of fast dissipation of the wave-packet. Nevertheless, one can see some indication of small partial revival of the wave-packet in the oscillations of P* stimulated emission in mutant LL131H and LL131H/LM160H/FM197H *Rba. sphaeroides* RCs as well as in native *Rba. sphaeroides* RCs (Figs. 2-4). For example, in the LL131H mutant the amplitude of the third and fourth oscillation peak is bigger than the amplitude of the second peak (Fig. 2). In the triple mutant the amplitude of fifth peak of the oscillations at 1.3-psec delay is markedly bigger than the amplitude of the third and especially the fourth peak (Fig. 3). In native RCs the amplitude of the fifth peak of the oscillations at 0.9 psec is markedly bigger than the amplitude of third and fourth peaks (Fig. 4). Similar features were noted in the oscillations of P* stimulated emission in pheophytin-modified *Rba. sphaeroides* RCs and in YM210W and YM210L mutant RCs to a less extent [18]. In all mentioned cases the revival of the wave-packet is observed in experiments at ~1-psec delay as it is in the calculations shown in Fig. 7a.

Inclusion of only one inharmonicity parameter α into the calculations does not provide satisfactory similarity of the $<x>(t)$ dependence with the experimental oscillations. Insertion of higher order parameters of inharmonicity β and γ remarkably improved qualitative similarity of the experimental and calculated oscillations and allows a coincidence of the frequencies of most of the modes from Fourier spectra of these oscillations (Fig. 7, b-e). As directly follows from (8), the modes from the Fourier spectrum of the $<x>(t)$ dependence becomes non-equidistant when β and γ are taken into account, which leads to considerable change in the behavior of this dependence. Quasi-chaotic oscillations with definite reference frequency are obtained in calculations instead of periodic revival of the wave-packet. Partial revival of the wave-packet takes place only once at 1-1.5-psec delay. By varying the β and γ parameters it is possible to obtain a condensation of the modes from the Fourier spectra with increasing frequency (Fig. 7d) or their rarefaction (Fig. 7, b, c, and e). In the experimental Fourier spectra of the oscillations of P* stimulated emission the increase of the distance between the modes (rarefaction) is observed with increasing frequency that is especially distinct for the most high-frequency modes. The energy levels E_n themselves can be condensed with increase in number n (Fig. 7, b and d) as well as can be rarer (Fig. 7c) with different sets of the β and γ parameters. In the last case their number are not formally limited in calculations. It is evident that in the case of rarefaction of the levels with increase of their numbers the Fourier spectra modes with higher frequencies are corresponding to the levels with larger numbers, and *vice versa*. Note that similar dependences

$\langle x \rangle$(t) with similar Fourier spectra are obtained both in the case of condensation of the energy levels with increase of their number (Fig. 7b) and in the opposite case (Fig. 7c). An intermediate case is shown in Fig. 7e, where the decrease of the distance between neighboring levels approximately down to 0 with increase of number n is followed by its further increase. In this case the Fourier spectrum of the $\langle x \rangle$(t) dependence consists of two sequences of modes inserted into each other. The first sequence is corresponding to the condensed E_n levels, and the second sequence to rare levels such that the modes from the two sequences alternate with each other. For this case there is characteristically the presence of the modes with frequencies as high as ~500 cm^{-1} in the Fourier spectra. A comparison of the values of inharmonicity parameters have been used in the calculations with the known values of the analogous parameters for diatomic molecules [33] suggests rather strong inharmonicity that is responsible for the wide frequency range from 10 to 500 cm^{-1} of spectral components of the oscillations.

A transition of a part of the wave-packet from the P* surface to the $P^+B_A^-$ surface takes place in the intersection area of the P* and $P^+B_A^-$ potential surfaces [38]. By the known formula of Landau–Zanier it is possible to evaluate the evolution of spectral components of the wave-packet motion at this transition:

$$p = 1-\exp(-2\pi V^2/(\hbar \mathrm{d}x/\mathrm{d}t \mid \mathrm{d}U_1/\mathrm{d}x - \mathrm{d}U_2/\mathrm{d}x|)), \quad (14)$$

where p is a probability of the transition from donor surface to acceptor surface when a particle passes a point of surface intersection with a speed $\mathrm{d}x/\mathrm{dt}$, V is energy of electron conjugation, $\mathrm{d}U_1/\mathrm{d}x$ and $\mathrm{d}U_2/\mathrm{d}x$ is curvature of the donor and acceptor surfaces at the point of their intersection [39]. It follows from (14) that the lower the particle speed, the higher the probability of its transition. According to (6), different parts of the wave-packet move with a speed that is proportional to their frequency: $\mathrm{d}\langle x \rangle/\mathrm{dt} \sim (\omega_{n+1}-\omega_n)$. The lower frequency $(\omega_{n+1}-\omega_n)$ corresponds to the higher probability for the part of the wave-packet with this frequency to transit to the other surface. The probability p is close to 1 if the speed is close to 0. So, a percentage of the low frequencies in the spectra of the wave-packet motion is higher for the acceptor surface than for the donor surface. Estimations show that for the lowest frequency mode (~20 cm^{-1}) of the Fourier spectrum of the P* band oscillations the transition probability p is 3-4 times higher than for the mode with frequency ~200 cm^{-1}. Just this effect of the low-frequency filtration is observed in the spectrum of the $P^+B_A^-$ state oscillations in many types of RCs [13-16, 18, 27]. The effect of low-frequency filtration is repeated again when the wave-packet transits from the $P^+B_A^-$ surface to the $P^+H_A^-$ surface, which leads to the domination of the modes with low frequencies ~20-70 cm^{-1} in the oscillations of the H_A absorption band at 760 nm [16]. Note that the inharmonicity of the P* surface causes location of low-frequency wave-packet components close to the walls of the potential well and location of high-frequency components near the bottom of the well when the energy levels are condensed with increase of their number (and *vice versa* when they become rarer). Therefore, the higher location of the intersection point of the surfaces above the bottom, the larger the percentage of low frequencies in the wave-packet that transits to the acceptor surface. Accounting for the inharmonicity of the acceptor potential can cause appearance of new modes in the spectrum of the motion of the wave-packet. A comparison of the oscillations from the P* band of native RCs (Fig. 4) with those from RCs of the triple mutant, in which electron transfer is negligible during first picoseconds after excitation (Fig. 3), gives an estimation of the forward transition probability of the wave-packet $p \sim 0.1$.

Therefore, inharmonicity of the potential energy surface of P* on which the nuclear wave-packet moves can explain the details of this motion. Even the simplest theoretical approach used in this work provides qualitative accordance of the Fourier spectra of the motion of wave-packet gravity center with experimental Fourier spectra of the oscillations in the P* emission band. The presence of inharmonicity in nuclear motions of such a complicated molecule as BChl is not a surprise. Mathematical modeling with consideration for changes of wave-packet form can be even more fruitful.

Finally, in this work the coherent effects accompanying primary charge separation were studied in the LL131H and LL131H/LM160H/FM197H mutant RCs from the purple bacterium *Rba. sphaeroides*. The oscillations caused by nuclear wave-packet motion along the P* potential energy surface were found in the kinetics of P* stimulated emission of both mutants at 940-950 nm. Charge separation is considerably retarded in these mutants; therefore, these oscillations reflect mostly vibrations inside the dimer P during several picoseconds after excitation. It was shown that the spectral and temporal features of the oscillations can be explained by inharmonicity of the P* potential surface.

The authors are grateful to A. Yu. Khmelnitsky for help in preparing RC samples.

This work was done with financial support of the Russian Academy of Sciences and the Russian Foundation for Basic Research (grant No. 11-04-00312).

REFERENCES

1. Shuvalov, V. A. (1990) *Primary Conversion of Light Energy in Photosynthesis* [in Russian], Nauka, Moscow.
2. Shuvalov, V. A. (2000) *Conversion of Light Energy in Primary Act of Charge Separation in Reaction Centers of Photosynthesis* [in Russian], Nauka, Moscow.

3. Kirmaier, C., and Holten, D. (1993) in *The Photosynthetic Reaction Center* (Deisenhofer, J., and Norris, J., eds.) Academic Press, San Diego, pp. 49-70.
4. Woodbury, N. W., and Allen, J. P. (1995) in *Anoxygenic Photosynthetic Bacteria* (Blankenship, R. E., Madigan, M. T., and Bauer, C. E., eds.) Kluwer Academic Publishers, Dordrecht, pp. 527-557.
5. Shuvalov, V. A., and Yakovlev, A. G. (2003) *FEBS Lett.*, **540**, 26-34.
6. Vos, M. H., Lambry, J.-C., Robles, S. J., Youvan, D. C., Breton, J., and Martin, J.-L. (1991) *Proc. Natl. Acad. Sci. USA*, **88**, 8885-8889.
7. Vos, M. H., Rappaport, F., Lambry, J.-C., Breton, J., and Martin, J.-L. (1993) *Nature*, **363**, 320-325.
8. Vos, M. H., Jones, M. R., Hunter, C. N., Breton, J., Lambry, J.-C., and Martin, J.-L. (1994) *Biochemistry*, **33**, 6750-6757.
9. Vos, M. H., Jones, M. R., Breton, J., Lambry, J.-C., and Martin, J.-L. (1996) *Biochemistry*, **35**, 2687-2692.
10. Stanley, R. J., and Boxer, S. G. (1995) *J. Phys. Chem.*, **99**, 859-863.
11. Sporlein, S., Zinth, W., and Wachtveitl, J. (1998) *J. Phys. Chem. B*, **102**, 7492-7496.
12. Streltsov, A. M., Vulto, S. I. E., Shkuropatov, A. Ya., Hoff, A. J., Aartsma, T. J., and Shuvalov, V. A. (1998) *J. Phys. Chem. B*, **102**, 7293-7298.
13. Yakovlev, A. G., Shkuropatov, A. Ya., and Shuvalov, V. A. (2000) *FEBS Lett.*, **466**, 209-212.
14. Yakovlev, A. G., and Shuvalov, V. A. (2000) *J. Chin. Chem. Soc.*, **47**, 709-714.
15. Yakovlev, A. G., Shkuropatov, A. Ya., and Shuvalov, V. A. (2002) *Biochemistry*, **41**, 2667-2674.
16. Yakovlev, A. G., Shkuropatov, A. Ya., and Shuvalov, V. A. (2002) *Biochemistry*, **41**, 14019-14027.
17. Vos, M. H., Rischel, C., Jones, M. R., and Martin, J.-L. (2000) *Biochemistry*, **39**, 8353-8361.
18. Yakovlev, A. G., Vasilieva, L. G., Shkuropatov, A. Ya., Bolgarina, T. I., Shkuropatova, V. A., and Shuvalov, V. A. (2003) *J. Phys. Chem. A*, **107**, 8330-8338.
19. Parson, W. W., Chu, Z. T., and Warshel, A. (1998) *Photosynth. Res.*, **55**, 147-152.
20. Allen, J. P., and Williams, J. C. (1995) *J. Bioenerg. Biomembr.*, **27**, 275-283.
21. Lin, X., Murchison, H. A., Nagarajan, V., Parson, W. W., Allen, J. P., and Williams, J. C. (1994) *Proc. Natl. Acad. Sci. USA*, **91**, 10265-10269.
22. Woodbury, N. W., Lin, S., Lin, X., Peloquin, J. M., Taguchi, A. K. W., Williams, J. C., and Allen, J. P. (1995) *Chem. Phys.*, **197**, 405-421.
23. Spidel, D., Jones, M. R., and Robert, B. (2002) *FEBS Lett.*, **527**, 171-175.
24. Rischel, C., Spiedel, D., Ridge, J. P., Jones, M. R., Breton, J., Lambry, J.-C., Martin, J.-L., and Vos, M. H. (1998) *Proc. Natl. Acad. Sci. USA*, **95**, 12306-12311.
25. Shuvalov, V. A., and Yakovlev, A. G. (1998) *Membr. Cell Biol. (Moscow)*, **12**, 563-569.
26. Shuvalov, V. A., Shkuropatov, A. Y., Kulakova, S. M., Ismailov, M. A., and Shkuropatova, V. A. (1986) *Biochim. Biophys. Acta*, **849**, 337-348.
27. Yakovlev, A. G., Vasilieva, L. G., Shkuropatov, A. Ya., and Shuvalov, V. A. (2009) *Biochemistry (Moscow)*, **74**, 1203-1210.
28. Hopfield, J. (1976) in *Phenomenes Electrique au Niveau des Membrane Biologique*, *29th Int. Congr. Soc. Chim. Phys.* (Roux, E., ed.) Elsevier, Amsterdam, pp. 471-492.
29. Marcus, S. A., and Sutin, N. (1985) *Biochim. Biophys. Acta*, **811**, 265-322.
30. Hu, Y., and Mukamel, S. (1990) in *Perspectives in Photosynthesis* (Jortner, J., and Pullman, B., eds.) Kluwer Academic Publishers, Amsterdam, pp. 171-184.
31. Moser, C. C., Keske, J. M., Warncke, K., Farid, R. S., and Dutton, P. L. (1992) *Nature*, **355**, 796-802.
32. Sokolov, A. A., and Ternov, I. M. (1970) *Quantum Mechanics and Atomic Physics* [in Russian], Prosveshchenie, Moscow.
33. Herzberg, H. (1949) *Vibrational and Rotational Spectra of Multiatoms Molecules* [Russian translation] (Sobolev, N. N., ed.) Inostrannaya Literatura, Moscow.
34. Klevanic, A. V., Ganago, A. O., Shkuropatov, A. Ya., and Shuvalov, A. V. (1988) *FEBS Lett.*, **237**, 61-64.
35. Glebov, L. O., and Eremin, V. V. (2008) *Russ. J. Phys. Chem.*, **82**, 684-689.
36. Yang, S., Cao, J., and Field, R. W. (2004) *J. Chem. Phys.*, **121**, 6599-6607.
37. Dantus, M., and Gross, P. (1998) *Encyclopedia Appl. Phys.*, **22**, 431-465.
38. Novoderezhkin, V. I., Yakovlev, A. G., van Grondelle, R., and Shuvalov, V. A. (2004) *J. Phys. Chem. B*, **108**, 7445-7457.
39. Landau, L. D., and Livshits, E. M. (1963) *Quantum Mechanics* [in Russian], Fizmatgiz, Moscow.